

Low-frequency and low-intensity ultrasound-mediated microvessel disruption enhance the effects of radiofrequency ablation on prostate cancer xenografts in nude mice

YU YANG*, WENKUN BAI*, YINI CHEN, WEI ZHANG, MEIWEN WANG and BING HU

Department of Ultrasound in Medicine, Shanghai Jiao Tong University Affiliated Sixth People's Hospital,
Shanghai Institute of Ultrasound in Medicine, Shanghai 200233, P.R. China

Received November 30, 2014; Accepted August 17, 2015

DOI: 10.3892/mmr.2015.4375

Abstract. The aim of the present study was to examine the impact of low-frequency, low-intensity ultrasound (US)-stimulated microbubbles (USMB) on radiofrequency ablation (RFA) in the treatment of nude mice with human prostate cancer xenografts. The tumor-bearing nude mice were divided into three groups: The USMB+RFA group was treated with USMB immediately followed by RFA, the RFA group was treated with RFA alone, and the control group remained untreated. The animals underwent enhanced US to calculate the tumor volumes, ablation volumes and ablation rates. Subsequently, the tumors were excised for hematoxylin and eosin staining, to identify necrosis in the tumors following the treatments, and immunohistochemical staining, to analyze the apoptotic index (AI), proliferative index (PI) and microvessel density (MVD) at 1, 4 and 7 days post-treatment. Each group contained five mice at each time-point. Necrosis was apparent in the center of the tumors in the treatment groups. Ablation lesion volumes of the USMB+RFA group were larger than those in the RFA group at 1 and 4 days post-treatment ($P=0.002$ and $P=0.022$, respectively), and the ablation rates of the USMB+RFA group were significantly higher, compared with the RFA group at the three time-points (all $P<0.001$). There were fewer apoptotic cells and more proliferative cells in the RFA group, compared with the control group 1, 4 and 7 days post-treatment (all $P<0.05$). The AI of the USMB+RFA group was higher than that of the control group and lower than that of the RFA group 1 day post-treatment ($P=0.034$ and $P=0.016$,

respectively). The PI of the USMB+RFA group was lower than that of the control group and higher than that of the RFA group 4 and 7 days post-treatment (all $P<0.05$). No significant differences were observed in MVD among the three groups throughout the experiment. In conclusion, exposure to USMB prior to RFA produced larger volumes of ablation, compared with treatment with RFA alone, and increased AI and reduced PI in the residual carcinoma cells induced by RFA.

Introduction

The morbidity rates of prostate cancer are estimated to be the highest of malignancies in American males, and is the second leading cause of tumor-associated mortality among American males, accounting for 27% (233,000 cases) of all newly diagnosed cancers in males and 10% (29,480 cases) of all cancer-associated mortality in American males in 2014 (1). Common treatment therapies include radical prostatectomy, radiation or radiotherapy (external beam, brachytherapy), chemotherapy and active surveillance (2). The majority of patients receive hormone therapy in the early stage, however, a substantial percentage of androgen-dependent types of cancer gradually become resistant to castration, and ultimately progress to a more aggressive and androgen-independent form (3,4). There are also disadvantages to other treatments, which include risks and injuries from surgery, systemic side effects following radiation and chemotherapy, and anxiety during surveillance (5,6). In addition, with prostate-specific antigen screening and transrectal ultrasonography becoming universal, and the development of magnetic resonance imaging and transrectal ultrasound (US)-guided prostate biopsy, the accuracy of diagnosis and localization has increased, increasing the number of small-sized and low-grade lesions of prostate carcinoma being diagnosed, particularly in young males (7). As a result, radiofrequency ablation (RFA) has emerged as an invasive therapy between radical approaches and active surveillance to manage small-sized, low-grade types of prostate cancer (7). RFA energy produces ionic or molecular friction and collision of particles, and delivers high-frequency energy to target tissues, ultimately inducing coagulative necrosis of tumor tissues (8,9). The minimal temperature required for complete tissue destruction is 55°C (8).

Correspondence to: Professor Bing Hu, Department of Ultrasound in Medicine, Shanghai Jiao Tong University Affiliated Sixth People's Hospital, Shanghai Institute of Ultrasound in Medicine, 600 Yi Shan Road, Shanghai 200233, P.R. China
E-mail: hubingedu@hotmail.com

*Contributed equally

Key words: low frequency ultrasound, radiofrequency ablation, microbubble, prostate carcinoma, tumor vasculature

Generally, RFA has been restricted to tumors measuring <3 cm in diameter, as RFA cannot achieve complete ablation for larger tumors (10). This has often been attributed to limitations in uneven energy deposition of RF heating in the tumor and the effects of blood flow into and out of the tumor (11). Vascular flow can cause heat dispersion through convection and reduce the volume of thermally induced coagulation, which has been referred to as the heat-sink effect (9). The heat-sink effect frequently leads to treatment failure in patients, and this unwanted effect can be accentuated when the tumor is hypervascular (9,12). In addition, heat loss can cause variability in lesion volume and shape (13). Furthermore, RFA affects the tumor microenvironment, and incomplete RFA may induce residual carcinoma cells to proliferate more rapidly and become more aggressive (14).

In recent years there has been an increase in investigations of a novel antivasculature approach, which uses low-frequency, low-intensity ultrasound-stimulated microbubbles (USMB) to disrupt tumor vasculature (15-17). Our previous study demonstrated that blood perfusion in human prostate cancer xenografts in nude mice can be effectively arrested for 2 h, which may be used to mitigate the effect of the heat sink. In addition, USMB has the capacity to promote apoptosis, and inhibit proliferation and angiogenesis in tumors (18,19), which may assist in reducing the number of over-proliferating residual carcinoma cells activated by incomplete thermal ablation. Therefore, it is hypothesized that this technology to reduce tumor blood flow may be used to enhance thermal ablation to treat castration-resistant prostate cancer.

To the best of our knowledge, the effects of USMB on RFA has not been previously reported. The present study hypothesized that USMB prior to RFA may yield results similar to those of surgery. A technique, which combines USMB prior to RFA may offer promise for the treatment of relatively large or hypervascular prostate tumors. In the present study, a subcutaneous transplanted model of human prostate cancer in nude mice was used to determine the involvement and effects of USMB in RFA.

Materials and methods

Cell lines and xenograft tumor model. The present study was approved by the Institutional Review Board of Shanghai Jiao Tong University Affiliated Sixth People's Hospital (Shanghai, China). The PC3 human androgen-independent prostate cancer cell line was obtained from the Cell Bank of the Chinese Academy of Sciences (Shanghai, China). The cells were cultured in DMEM medium (GE Healthcare Life Sciences, Logan, UT, USA), which was added with 10% fetal bovine serum (Zhejiang Tianhang Biological Technology Co., Hangzhou, China) in an incubator with 5% CO₂ at 37°C. When the cells reached 80% confluence, they were washed with phosphate-buffered saline (PBS), trypsinized (trypsin: Ginuo Biomedical Technology Co., Ltd., Hangzhou, China) and centrifuged at 150 x g for 5 min at 25°C. Subsequently, the cells were resuspended in PBS and the final viable cell solution was estimated at a concentration of 1x10⁷ cells per 100 µl.

A total of 50 male Balb-c nude mice (5-6 weeks old; weight, 20-25 g) were purchased from Shanghai Super-B&K Laboratory Animal Corp., Ltd. (Shanghai, China) and raised

in the Animal Laboratory of Shanghai Jiao Tong University Affiliated Sixth People's Hospital. The mice were housed in 10 cages (five mice per cage) at a temperature of 25°C, under a 12-h light/dark cycle. The mice were fed with sufficient chow and water for one week prior to being injected with the PC3 prostate cancer cells. Each procedure, including the establishing of the animal model and therapeutic treatment, was performed under general anesthesia via an intraperitoneal injection of 50 mg/kg of 1.5% pentobarbital sodium (Merck Millipore, Darmstadt, Germany) and local sterilization. Each mouse was subcutaneously inoculated with 1x10⁷ PC3 cells into the right flank. Subsequently, the mice were maintained under specified pathogen-free conditions, and were observed for weight gain, mental status and tumor size at 2-day intervals. Experiments were initiated 18 days later, when the tumor size was ~8 mm in maximum diameter, in 48 nude mice (two mice were excluded from the experiment, as tumors had not established in them). Of these 48 mice, 45 were recruited for the subsequent experiment, as three mice were excluded due to perfusion defects, observed by enhanced ultrasonography (EUS), in the center of the tumors 18 days after PC3 cell inoculation, which indicated necrosis.

Treatment procedures. The animals were randomly divided into three groups of 15 animals: The USMB+RFA group was treated with combined therapy (USMB followed by RFA), the RFA group was treated with RFA alone, and the control group remained untreated. Following treatment, the animals underwent EUS to evaluate the tumor and ablation volumes, and the tumors were surgically excised for hematoxylin and eosin (HE; Beijing Leagene Biotech Co., Ltd., Beijing, China) staining, tumor apoptosis analysis, and the detection of cell proliferation and angiogenesis, with five mice per group, at 1, 4 and 7 days following treatment. Subsequently, the five mice in each group were sacrificed by an overdose injection of sodium pentobarbital (150 mg/kg). Treatment with USMB alone was excluded from the present study for three reasons. Firstly, USMB alone can inhibit tumor growth, however, tumor growth occurs at a slower rate (18,19), which was further confirmed in our previous studies (20), therefore the combination of USMB with other therapies is suggested to treat cancer, rather than alone. Secondly, RFA is able to achieve complete ablation of tumors measuring <3 cm in diameter, however, eradication of larger tumors and avoiding proliferation of residual tumor cells remains a challenge. Finally, the present study aimed to investigate how to enhance the curative effect of RFA, and hypothesized that USMB prior to RFA may overcome the limitations of RFA.

MB treatment. Albumin-coated MBs, also known as perfluoropropane-albumin microsphere injection (RunKun Pharmaceutical Co., Yueyang, China), were used for EUS and therapeutic application. The MBs had a mean diameter of 3.4 µm, with 99% of the particles <10 µm in diameter and an MB concentration of 6.5x10⁸/ml. The MBs were agitated gently for ~20 sec to produce a milky white suspension. For EUS, a bolus injection of 0.10 ml MB was injected into the caudal veins of the mice. To induce vessel blocking, a bolus injection of 0.20 ml MB was administered, via the caudal veins, for each treatment.

USMB treatment. The low frequency US equipment was manufactured by the Shanghai Institute of Ultrasound in Medicine (Shanghai, China). The diameter of the therapeutic US transducer was 20 mm, which covered the entire tumor. The therapeutic parameters were determined according to the orthogonal experimental design of our previous study (21): Frequency, 20 kHz; acoustic intensity, 1 W/cm²; duty cycle, 40% (2 sec on/3 sec off); irradiation duration, 3 min. The intermittent working mode allowed the MBs to refill following the destruction of every MB. Following intravenous injection of the MBs (0.20 ml), the tumors were insonated percutaneously with low-frequency low-intensity US for 3 min.

RFA procedure. RFA was performed using a 480-kHz VIVA RF generator (Star Med Co., Ltd., Goyang-si, Korea). An 18-gauge internally cooled electrode with a 5-mm-tip (Star Med Co., Ltd.) was inserted percutaneously into the tumor. RFA was applied at 5 W in a continuous mode for 12 sec. These RFA parameters were selected in preliminary experiments to induce RF ablation without complete destruction of the tumor, thereby permitting the evaluation of ablation volumes and histological analysis of the peripheral untreated tumor. The treatment duration and electrode tip temperature were monitored throughout the RFA procedure.

Calculation of tumor and ablation volume. A commercially available US imaging system (Mylab90; Esaote SpA, Genoa, Italy), equipped with an LA522 high frequency linear array probe (Esaote SpA), was used for EUS. Dual-frame imaging, combining two-dimensional (2-D) and contrast modality was performed using a low mechanical index (0.05). The depth, frequency and other US conditions were the same during all EUS procedures. The recorded diameters of the tumor and ablation lesion in the EUS images were based on the consensus of two observers. The tumor and ablation volumes were calculated according to the following formula: Tumor or ablation volume (mm³) = (a x b²)/2, where a and b represent the longest and the shortest diameters of the measured tumor (or volumes of ablation), respectively. Tumor ablation was calculated using the following formula: Rate of tumor ablation (%) = ablation volume / tumor volume x 100%.

Sample collection and pathological examination. The harvested tumor specimens were fixed in 10% neutral formalin (Nanchang Yulu Experimental Equipment Co., Ltd., Nanchang, China) for 24 h, following which the tissues were embedded in paraffin (Leica Microsystems GmbH, Wetzlar, Germany). The largest sections (5-μm thick) were obtained for HE and immunohistochemical staining to analyze tumor apoptosis, proliferation and angiogenesis. A pathologist, blinded to the experimental procedures, evaluated morphological tissue changes under a light microscope (CX41; Olympus Corporation, Tokyo, Japan).

Apoptosis of the tumor cells was determined using terminal deoxynucleotidyl transferase-mediated deoxyuridine triphosphate nick-end labeling (TUNEL), using a commercially available *In situ* Cell Death Detection kit (POD; Roche Diagnostics GmbH, Mannheim, Germany). Slides were counterstained with hematoxylin, and the total number of tumor cell nuclei and TUNEL-positive cell nuclei were

counted (magnification, x400). The apoptotic cells were those exhibiting DNA fragmentation and nuclei stained brown or tan. At least five randomly-selected, non-overlapping fields per tumor were analyzed, containing at least 500 nuclei for TUNEL staining. Apoptotic index (AI) was defined as the ratio of TUNEL-positive tumor cell nuclei to the total tumor cell nuclei, expressed as percentage.

Immunohistochemical quantification of the proliferation of tumor cells was determined using rabbit anti-human Ki-67 monoclonal antibody (1:500; cat. no. ab92742; Abcam, Cambridge, UK). Antigen retrieval was performed by boiling in 10 mmol/L sodium citrate buffer for 15 min. The non-specific binding sites were blocked with goat serum (Wuhan Boster Biological Technology, Ltd., Wuhan, China) for 30 min. The rabbit anti-Ki-67 antibody was applied to slides and incubated overnight at 4°C. The slides were then incubated with goat anti-rabbit antibody (1:500; cat. no. ZB-2301; OriGene Technologies, Beijing, China) for 30 min at 37°C. The primary antibody was replaced by PBS, which served as a negative control. The slides were counterstained with hematoxylin, and the total number of tumor cell nuclei and Ki-67-positive cell nuclei was counted (magnification, x400). Ki-67-positive cell nuclei were stained brown or tan. A total of five randomly selected, non-overlapping fields were analyzed, with at least 500 nuclei counted from each section for Ki-67 staining. Proliferative index (PI) was defined as the ratio of Ki-67 positive tumor cell nuclei to total tumor cell nuclei, expressed as percentage.

Quantification of tumor angiogenesis in the tumor tissue was determined using rabbit anti-mouse CD34 monoclonal antibody (1:250; cat. no. ab81289; Abcam). Antigen retrieval was performed by boiling in 10 mmol/L sodium citrate buffer for 15 min. The non-specific binding sites were blocked with goat serum (Wuhan Boster Biological Technology, Ltd., Wuhan, China) for 30 min. The rabbit anti-CD34 antibody was applied to slides and incubated overnight at 4°C. The slides were then incubated with goat anti-rabbit antibody (1:1,000; cat. no. ZB-2301; OriGene Technologies) for 30 min at 37°C. The primary antibody was replaced by PBS, which served as a negative control. The slides were counterstained with hematoxylin. Blood vessels were stained brown. CD34 staining of the blood vessels was observed under a microscope (magnification, x400). For each slide, microvessel density (MVD) was calculated as the number of CD34-positive vessels in five randomly-selected, non-overlapping fields.

Statistical analysis. All data are expressed as the mean ± standard deviation. SPSS 19.0 (IBM SPSS, Armonk, NY, USA) was used to analyze data. Repeated measures analysis of variance was used for comparisons of differences in tumor volume, ablation volume, ablation rate, AI, PI and MVD between the different time-points within a single group, and a least significant difference (LSD) test was used for multiple comparisons. One-way analysis of variance was used for comparisons of differences in tumor volume, AI, PI and MVD between groups at the same time-point, and the LSD test was used for multiple comparisons. An independent sample *t*-test was used for comparisons of differences in tumor ablation volume and ablation rate between two treatment groups at the same time-point. P<0.05 was considered to indicate a statistically significant difference.

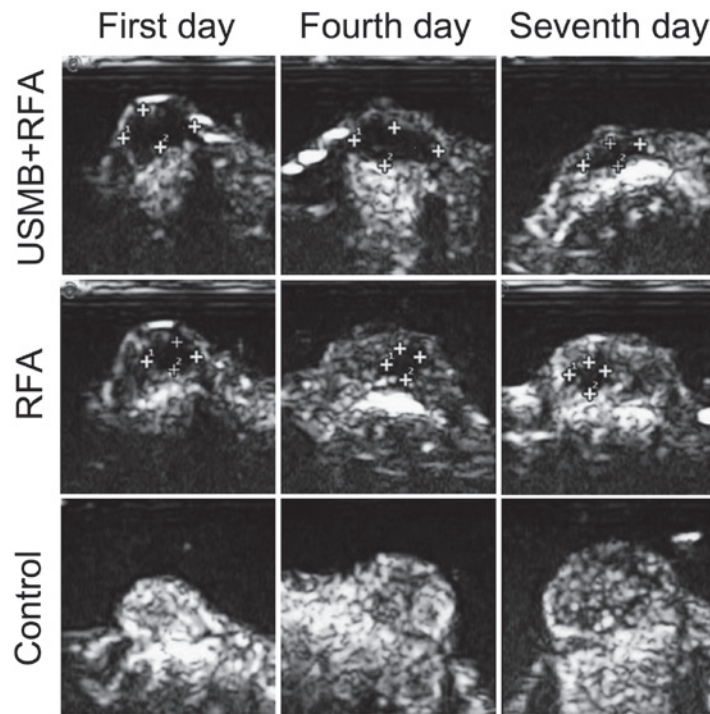


Figure 1. EUS of tumors in the USMB+RFA, RFA and control groups. The contrast images were determined using two-dimensional ultrasonography of the largest section of the tumor. All xenografts exhibited marked and homogenous enhancement in EUS prior to treatment. Following treatment, the regions of ablation lesions in the two treatment groups were readily distinguishable from the residual tumor tissues, as they revealed no enhancement. However, in the control group, the tumors displayed marked enhancement. The cross symbols indicate the boundaries to measure the longest and shortest diameters of the ablation areas. EUS, enhanced ultrasonography; USMB, ultrasound-stimulated microbubbles; RFA, radiofrequency ablation.

Results

Tumors were established in all animals following the inoculation of PC-3 cells. All animals survived the procedures until the designated time-point of euthanasia following the procedure. The tumor and ablation volumes of RFA with or without USMB were evaluated using ultrasonography. To assess differences in histology between the three groups, tumor specimens were examined using HE staining and immunohistochemical staining for apoptosis (TUNEL assay), proliferation (Ki-67) and angiogenesis (MVD). HE indicated necrosis in the center of the tumors from the treatment groups, while no obvious necrosis was observed in the control group. This confirmed the efficacy of the RFA alone and USMB+RFA treatment methods.

Tumor and ablation volume. The implanted tumors were observed to be spherical, elliptical or nodular in shape and were well-defined and homogeneously hypoechoic in the 2-D ultrasonography (Fig. 1). All xenografts demonstrated marked and homogenous enhancement in EUS prior to treatment. Following treatment, the regions of the ablation lesions in the two treatment groups were readily distinguishable from the residual tumor tissues, as perfusion defects were visible in the EUS.

The tumor volumes in the days subsequent to treatment are shown in Fig. 2A. No significant differences in the three groups were observed 1 day following treatments. Significant differences in tumor volumes were observed among the three groups ($P < 0.05$; Fig. 2A) at 4 days post-treatment. Tumor volumes were reduced by treatment with USMB combined

with RFA, while the RFA group exhibited larger tumor volumes, compared with the control group ($P < 0.001$ and $P = 0.037$, respectively; Fig. 2A). On day 7, the tumor volumes were smaller in the USMB+RFA group, compared with the other two groups ($P < 0.001$; Fig. 2A). The tumors treated with RFA were smaller than those in the control group, although this difference was not significant ($P = 0.165$; Fig. 2A). Only the combination of USMB and RFA produced measurable tumor volume reduction, whereas tumor volumes in the RFA group and control group increased over time ($P < 0.05$; Fig. 2A).

At 1 and 4 days post-treatment, a larger average ablation lesion volume was observed in the USMB+RFA group, compared with the RFA group ($P = 0.002$ and $P = 0.022$ at 1 and 4 days post-treatment, respectively; Fig. 2B). In the two treatment groups, ablation volumes decreased with time, although the differences were only significant in the USMB+RFA group (Fig. 2B).

The ablation rates were higher in the USMB+RFA group compared with the RFA group 1, 4 and 7 days following treatment ($P < 0.001$; Fig. 2C). In the USMB+RFA group, ablation rates increased with time, however, the differences between the different time-points were not significant ($P > 0.05$; Fig. 2C). In the RFA group, ablation rates decreased with time, and on day 1 post-treatment the rates were significantly higher, compared with those on days 4 and 7 post-treatment ($P = 0.040$ and $P = 0.016$, respectively; Fig. 2C).

Tumor apoptosis. The present study performed TUNEL assays (Fig 3) of the subcutaneous tumors to conform the apoptotic effects in the different groups. Treatment with RFA alone and with USMB+RFA resulted in decreases in AI, compared with

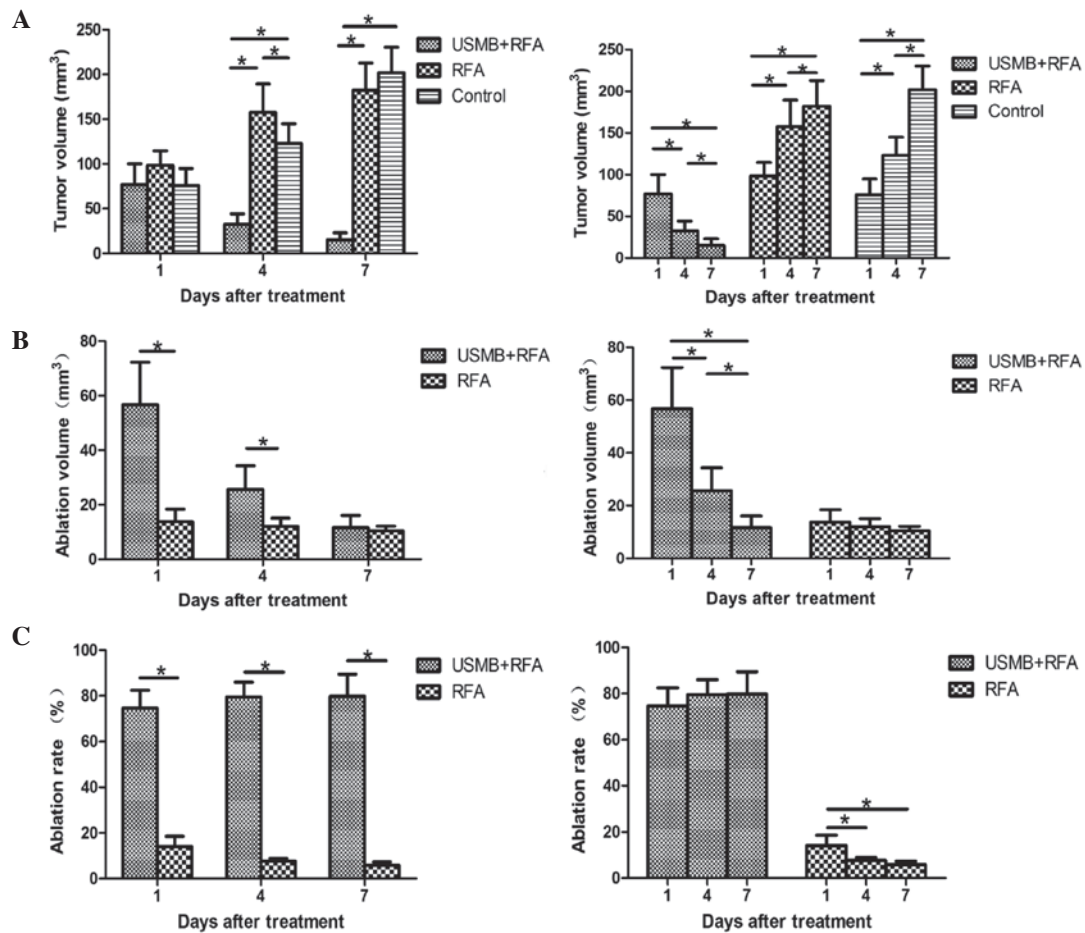


Figure 2. Tumor volumes and ablation volumes in the USMB+RFA group, RFA group and control group, and ablation rates in the USMB+RFA and RFA groups. (A) Tumor volumes in the USMB+RFA, RFA and control groups. (B) Ablation volumes in the USMB+RFA and RFA groups. (C) Ablation rates in the USMB+RFA and RFA groups. *P<0.05. Data are expressed as the mean \pm standard deviation. USMB, ultrasound-stimulated microbubbles; RFA, radiofrequency ablation.

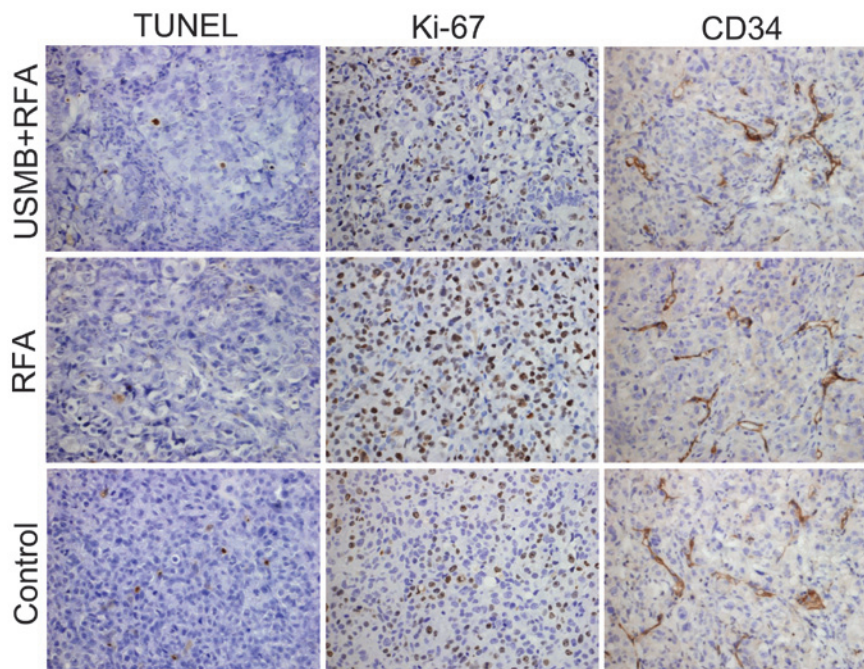


Figure 3. Representative images of TUNEL and immunohistochemical staining of Ki-67 and CD34 in the USMB+RFA, RFA and control groups 1 day post-treatment. Compared with the control and USMB+RFA groups, treatment with RFA alone resulted in less TUNEL-positive cells. Furthermore, fewer Ki-67-positive cells were observed in the control group, compared with the two treatment groups. The difference in CD34 staining between the three groups was not significant. Slides were counterstained using hematoxylin. Magnification, x400. TUNEL, terminal deoxynucleotidyl transferase-mediated deoxyuridine triphosphate nick-end labeling; USMB, ultrasound-stimulated microbubbles; RFA, radiofrequency ablation.

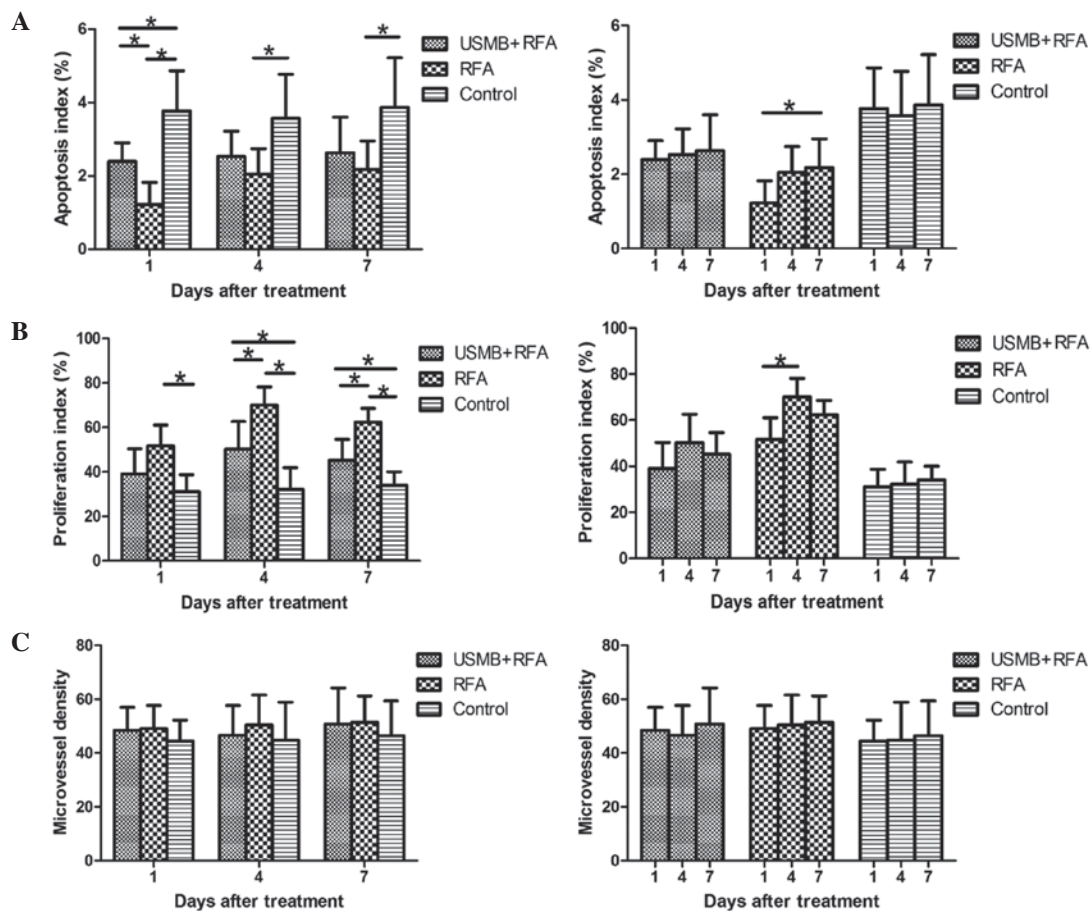


Figure 4. Apoptotic index, proliferation index and microvessel density in the USMB+RFA, RFA and control groups. (A) Apoptosis index in the USMB+RFA, RFA and control groups. (B) Proliferation index in the USMB+RFA, RFA and control groups. (C) Microvessel density in the USMB+RFA, RFA and control groups. * $P < 0.05$. Data are expressed as the mean \pm standard deviation. USMB, ultrasound-stimulated microbubbles; RFA, radiofrequency ablation.

the control ($P < 0.001$ and $P = 0.016$, respectively; Fig. 4A) and AI decreased more significantly in the RFA group, compared with the USMB+RFA group at 1 day post-treatment ($P = 0.034$; Fig. 4A). At 4 and 7 days post-treatment, the AI was lower in the RFA group, compared with the control ($P = 0.020$ and $P = 0.027$, respectively; Fig. 4A) and the USMB+RFA group, however, the differences between the RFA and USMB+RFA groups were not significant ($P = 0.412$ and $P = 0.506$, respectively; Fig. 4A). The AI of the RFA group increased over time, however, only the difference between days 1 and 7 was statistically significant ($P = 0.048$; Fig. 4A). The changes in AI in the USMB+RFA and control groups over time were not significant ($P > 0.05$; Fig. 4A).

Immunohistochemical staining of cell proliferation and angiogenesis. Immunohistochemical staining of Ki-67 in the subcutaneous tumors (Fig. 3) was performed to examine the proliferative effects in the different groups. At 1 day post-treatment, the PI values were higher in the control group, compared with the two treatment groups, although only the difference with the RFA group was significant ($P = 0.005$; Fig. 4B). The PI of the tumors treated with RFA were lower than those in the USMB+RFA group, however, the difference was not significant ($P = 0.058$; Fig. 4B). Significant differences in PI were observed among the three groups 4 and 7 days post-treatment, as PI was higher in the USMB+RFA group,

compared with that in the control, whereas the RFA exhibited a higher PI, compared with the USMB+RFA group at 4 and 7 days post-treatment ($P < 0.05$; Fig. 4B). The PI of the RFA group peaked 4 days following treatment, however only the difference between days 1 and 4 was statistically significant ($P = 0.013$; Fig. 4B). The PI changes in the USMB+RFA and control groups over time were not significant (Fig. 4B).

To determine the effects of treatment on tumor angiogenesis, immunohistochemical staining of CD34 in the tumors was performed to quantify MVD. No significant differences were observed among the three groups throughout the experiment. The MVD in the RFA group was higher than those in the USMB+RFA and control groups at the three time-points, however, this was not significant ($P > 0.05$; Fig. 4C).

Discussion

Triggered by the increasing incidence of small-volume and low-grade foci of prostate cancer, and in investigating alternatives for patients unfit for radical prostatectomy and surveillance, RFA has been considered a promising treatment modality in animal experiments and clinical trials (7,22,23). However, RFA is susceptible to the heat-sink effect of flowing blood, which affects the therapeutic effect of RFA, by decreasing heat-induced coagulative necrosis, constituting a serious problem often leading to local recurrences following

ablation, particularly in large and hypervascular tumors (9-12). Thermal energy is conducted from the tip of an electrode to the surrounding tissue and is attenuated during conduction, therefore, cells at the edge of the tumor may survival sub-lethal injury (14). In addition, tumor perfusion and blood perfusion close to the tumor may affect the volume and contour of the ablation lesion (13). Therefore, complete ablation is not always achieved for large or hypervascular tumors, and RFA appears to require re-ablations to achieve its desired effect.

To solve this problem, the combining of RFA with various methods to relieve the heat-sink effect have provided promising results (9,11,24). These methods include pharmaceutical agents, transcatheter arterial embolisation (TAE) and transcatheter arterial chemoembolization (TACE). TAE and TACE have been used prior to RFA, which can lead to a larger ablation volume and more predictable and reproducible lesion shape, compared with the lesions created with RFA alone, particularly in tumors with rich blood flow (9,13). In addition, the size of the ablation lesion in the absence of blood perfusion is not affected by the method of flow blockage (13). However, it is difficult to completely embolize the tumor-feeding vessels due to the complexity of the blood supply and variation of blood vessel distribution (25).

As tumor blood vessels are weaker in structure and less competent than those in normal tissues (26), there is significant interest in developing techniques that target this neovasculture in order to reduce the heat-sink effect. In our previous study, blood perfusion in human prostate cancer xenografts in nude mice was effectively arrested for 2 h (unpublished data), which may be used to mitigate the effect of heat-sink to enhance thermal ablation. In the present study, as expected, ablation lesion volumes were significantly larger when RFA was combined with USMB, compared with treatment with RFA alone, although the differences were only significant 1 and 4 days post-treatment. As for tumor volume, the volumes in the USMB+RFA group were smaller than those in the RFA group, although the differences were only significant 4 and 7 days post-treatment. Therefore, the ablation rates in the USMB+RFA group were significantly higher than those in the RFA group throughout the experiment.

The mechanism underlying the cessation of tumor perfusion are predominantly vessel rupture, intravascular thrombosis and oppression of surrounding edema. Tumor blood perfusion can be blocked to different degrees using high intensity focused US (HIFU) and low-frequency US (17,27,28). With the presence of MBs, this vascular disruption effect can be operated at low acoustic intensity, and overcomes the thermal adverse effects of HIFU ablation (19). The antivasular effect is promising and reproducible. It has been demonstrated that thermal, mechanical (cavitation and other nonlinear mechanisms) and sonochemical effects are likely to contribute to the antivasular activities (26). These acoustic mechanisms may act either directly damage vascular structure or indirectly by inducing tissue response to the thermal, mechanical or sonochemical effects (26). Inertial cavitation and its corresponding effects are considered to be the dominant mechanisms underlying the microvessels damage (17,29). Acoustic cavitation is defined as the formation, growth, oscillation and collapse of bubbles under the effect of an ultrasonic wave in a liquid medium (30). Acoustic cavitation is divided into stable and

transient cavitation. Bubbles pulsating over numerous acoustic propagation cycles without collapse is stable cavitation, whereas transient cavitation is intense and fast bubble expansion over several acoustic wave cycles, leading to the eventual collapse into smaller bubbles (31,32). In US, when bubbles pass through blood vessels, they growth and contract in response to acoustic waves in accordance with the changing acoustic pressure over time, and these volumetric oscillations are important in therapeutic action (33). In stable cavitation, the oscillation of the bubbles can trigger the surrounding fluid to flow close to the pulsating bubbles, termed microstreaming (34). Microstreaming imposes a large shear stress on nearby vascular epithelial cells, and at high enough stresses, these endothelial cells eventually detach from the vessel wall (35). In addition, in stable cavitation, radiation forces can push bubbles in the direction of wave propagation, which can exert an effect on the endothelium (36). Above a particular threshold, in the transient cavitation stage, the bubble oscillation becomes so powerful that the bubbles eventually collapse, inducing local high temperatures and high pressures, and producing free radicals in the surrounding blood (37). These effects result in a shock wave. If the bubbles collapse close to a blood vessel wall, the shock wave may create liquid jets that impinge upon the vessel, creating poking holes on the vessel wall (38). Therefore, the various expansion, oscillation and collapse of the bubbles and the resultant microstreaming, shock wave and fluid jets result in microvessels distention, invagination and ultimately vessel rupture (29,38-41).

The necessity of increasing ablation volume is also induced by incomplete thermal ablation and may stimulate the proliferation of residual tumor cells (14). Several studies have reported that residual tumor cells following RFA may become more aggressive (14,42,43). In the present study, the proliferation-promoting effect of RFA was elucidated by the tumor volume and histopathological findings, compared with the control group. At 4 days post-treatment, the tumor volumes in the RFA group were larger than those in the control. There were fewer apoptotic cells and more proliferative cells in the RFA group, compared with the control group 1, 4 and 7 days post-treatment. This hyperproliferation may have been caused by increased hypoxia, cytokines, heat-shock proteins and influx of inflammatory cells at areas surrounding the ablated region (14,44). In particular, hypoxia in residual tumor tissues appears to be an important factor in over-proliferation (43). Hypoxic stress caused by RFA is less severe and prolonged, and residual tumour cells tolerate this injury, as it leads to the activation of cell signal transduction, which allow cells to undergo adaptive changes promoting survival (43,44). In the USMB+RFA group, fewer apoptotic cells were observed, compared with the control, however, more apoptotic cells were observed, compared with the RFA group 1 day following treatment. In addition, there was more proliferative cells in the USMB+RFA group, compared with the control, but fewer proliferative cells, compared with the RFA group at 4 and 7 days post-treatment. These results demonstrated that, although USMB+RFA reduced apoptosis and stimulated proliferation in the residual carcinoma cells, it assisted in reducing the degree of the proliferation-promoting effect in RFA. The present study hypothesized that the combination of USMB and RFA induced more lethal effect on the cells prior to their initiation of adaptive changes, therefore, the number of viable

tumor cells in a hypoxic microenvironment decreased. In addition, USMB itself has the capacity to promote apoptosis, and inhibit proliferation and angiogenesis in tumors (18,19). In the present study, the MVD in the RFA group was higher than that in the USMB+RFA group at the three time-points, although without statistical significance. The reason for this may be that tumor angiogenesis requires longer than the 7 days following treatment. As hyperproliferation following incomplete RFA can facilitate the recurrence of tumors, USMB prior to RFA offers promise for use in clinical practice.

The results of the present study suggested that the benefit of combination therapy may be due to two aspects. USMB prior to RFA may increase tumor ablation volume and ablation rate by decreasing tumor blood flow and the vascular-mediated tissue cooling effect. Secondly, USMB prior to RFA increases AI and reduce PI in the residual carcinoma cells induced by RFA. Therefore, the combined therapy is beneficial, compared with RFA alone, due to a synergistic effect of the two types of therapy.

However, there were a number of limitations to the present study. Firstly, the human prostate tumors were grown in nude mice subcutaneously, however, the microenvironments within and surrounding the tumors are different from those grown in clinical cases. However, prostate cancer cells can only be grown in nude mice in animals, and it enables accurate surgical removal of tumors inoculated subcutaneously. Secondly, the present study used a survival end point of only 7 days. Whether the therapeutic effects change in the long term, and the effects on long-term survival rates remain to be elucidated, but are difficult to determine in this delicate model.

In conclusion, the present study demonstrated that USMB prior to RFA produced larger volumes of ablation than RFA alone, and increased AI and reduced PI in the residual carcinoma cells induced by RFA. USMB prior to RFA is likely to have significance in clinical application as a standard treatment in the future, not only for prostate cancer, but for various types of cancer, including hepatocellular carcinoma and renal carcinoma, particularly for large, hypervascular tumors.

Acknowledgements

The authors would like to thank RunKun Pharmaceutical Co. for providing the perfluoropropane-albumin microsphere injection. The authors would also like to thank Star Med Co., Ltd. for providing the RF generator and electrode. This study was supported by the National Natural Science Foundation of China (grant nos. 81271597 and 81401421).

References

- Siegel R, Ma J, Zou Z and Jemal A: Cancer statistics, 2014. *CA Cancer J Clin* 64: 9-29, 2014.
- Fung-Kee-Fung SD, Porten SP, Meng MV and Kuettel M: The role of active surveillance in the management of prostate cancer. *J Natl Compr Canc Netw* 11: 183-187, 2013.
- Goldberg AA, Titorenko VI, Beach A and Sanderson JT: Bile acids induce apoptosis selectively in androgen-dependent and -independent prostate cancer cells. *PeerJ* 1: e122, 2013.
- Pienta KJ and Smith DC: Advances in prostate cancer chemotherapy: A new era begins. *CA Cancer J Clin* 55: 300-318; quiz 323-325, 2005.
- Penson DF: Quality of life after therapy for localized prostate cancer. *Cancer J* 13: 318-326, 2007.
- Bul M, Zhu X, Valdagni R, Pickles T, Kakehi Y, Rannikko A, Bjartell A, van der Schoot DK, Cornel EB, Conti GN, *et al*: Active surveillance for low-risk prostate cancer worldwide: the PRIAS study. *Eur Urol* 63: 597-603, 2013.
- Bozzini G, Colin P, Nevoux P, Villers A, Mordon S and Bétrouni N: Focal therapy of prostate cancer: Energies and procedures. *Urol Oncol* 31: 155-167, 2013.
- Djavan B, Zlotta AR, Susani M, Heinz G, Shariat S, Silverman DE, Schulman CC and Marberger M: Transperineal radiofrequency interstitial tumor ablation of the prostate: Correlation of magnetic resonance imaging with histopathologic examination. *Urology* 50: 986-992, 1997.
- Yoon SK, Choi JC, Cho JH, Oh JY, Nam KJ, Jung SI, Kwon HC, Kim DC and Rha SH: Radiofrequency ablation of renal VX2 tumors with and without renal artery occlusion in a rabbit model: Feasibility, therapeutic efficacy and safety. *Cardiovasc Intervent Radiol* 32: 1241-1246, 2009.
- Morimoto M, Sugimori K, Shirato K, Kokawa A, Tomita N, Saito T, Tanaka N, Nozawa A, Hara M, Sekihara H, *et al*: Treatment of hepatocellular carcinoma with radiofrequency ablation: Radiologic-histologic correlation during follow-up periods. *Hepatology* 35: 1467-1475, 2002.
- Mostafa EM, Ganguli S, Faintuch S, Mertyna P and Goldberg SN: Optimal strategies for combining transcatheter arterial chemo-embolization and radiofrequency ablation in rabbit VX2 hepatic tumors. *J Vasc Interv Radiol* 19: 1740-1748, 2008.
- Lee JJ, Kim YI, Kim KW, Kim DH, Ryoo I, Lee MW and Chung JW: Radiofrequency ablation combined with transcatheter arterial embolisation in rabbit liver: investigation of the ablation zone according to the time interval between the two therapies. *Br J Radiol* 85: e987-e994, 2012.
- Chang I, Mikityansky I, Wray-Cahen D, Pritchard WF, Karanian JW and Wood BJ: Effects of perfusion on radiofrequency ablation in swine kidneys. *Radiology* 231: 500-505, 2004.
- Kroeze SG, van Melick HH, Nijkamp MW, Kruse FK, Kruijsen LW, van Diest PJ, Bosch JL and Jans JJ: Incomplete thermal ablation stimulates proliferation of residual renal carcinoma cells in a translational murine model. *BJU Int* 110: E281-E286, 2012.
- Hwang JH, Brayman AA, Reidy MA, Matula TJ, Kimmey MB and Crum LA: Vascular effects induced by combined 1-MHz ultrasound and microbubble contrast agent treatments in vivo. *Ultrasound Med Biol* 31: 553-564, 2005.
- Wood AK, Bunte RM, Price HE, Deitz MS, Tsai JH, Lee WM and Sehgal CM: The disruption of murine tumor neovasculature by low-intensity ultrasound-comparison between 1- and 3-MHz sonication frequencies. *Acad Radiol* 15: 1133-1141, 2008.
- Liu Z, Gao S, Zhao Y, Li P, Liu J, Li P, Tan K and Xie F: Disruption of tumor neovasculature by microbubble enhanced ultrasound: A potential new physical therapy of anti-angiogenesis. *Ultrasound Med Biol* 38: 253-261, 2012.
- Shen ZY, Shen E, Diao XH, Bai WK, Zeng MX, Luan YY, Nan SL, Lin YD, Wei C, Chen L, *et al*: Inhibitory effects of subcutaneous tumors in nude mice mediated by low-frequency ultrasound and microbubbles. *Oncol Lett* 7: 1385-1390, 2014.
- Wang Y, Hu B, Diao X and Zhang J: Antitumor effect of microbubbles enhanced by low frequency ultrasound cavitation on prostate carcinoma xenografts in nude mice. *Exp Ther Med* 3: 187-191, 2012.
- Yang Y, Bai W, Chen Y, Nan S, Lin Y and Hu B: Low-frequency low-intensity ultrasound mediated microvessel disruption combined with docetaxel to treat prostate carcinoma xenografts in nude mice: A new type of chemoembolization. *Oncol Lett* (In press).
- Yang Y, Bai W, Chen Y, Lin Y and Hu B: Optimization of low-frequency low-intensity ultrasound mediated microvessel disruption on prostate cancer xenografts in nude mice by orthogonal experimental design. *Oncol Lett* (In press).
- Djavan B, Zlotta AR, Susani M, Heinz G, Shariat S, Silverman DE, Schulman CC and Marberger M: Transperineal radiofrequency interstitial tumor ablation of the prostate: correlation of magnetic resonance imaging with histopathologic examination. *Urology* 50: 986-983, 1997.
- McGahan JP, Griffey SM, Budenz RW and Brock JM: Percutaneous ultrasound-guided radiofrequency electrocautery ablation of prostate tissue in dogs. *Acad Radiol* 2: 61-65, 1995.
- Nakasone Y, Ikeda O, Kawanaka K, Yokoyama K and Yamashita Y: Radiofrequency ablation in a porcine kidney model: Effect of occlusion of the arterial blood supply on ablation temperature, coagulation diameter and histology. *Acta Radiol* 53: 852-856, 2012.

25. Duan X, Zhou G, Zheng C, Liang H, Liang B, Song S and Feng G: Heat shock protein 70 expression and effect of combined transcatheter arterial embolization and radiofrequency ablation in the rabbit VX2 liver tumour model. *Clin Radiol* 69: 186-193, 2014.
26. Levenback BJ, Sehgal CM and Wood AK: Modeling of thermal effects in antivasular ultrasound therapy. *J Acoust Soc Am* 131: 540-549, 2012.
27. Wu F, Chen WZ, Bai J, Zou JZ, Wang ZL, Zhu H and Wang ZB: Tumor vessel destruction resulting from high-intensity focused ultrasound in patients with solid malignancies. *Ultrasound Med Biol* 28: 535-542, 2002.
28. Wood AK, Ansaloni S, Ziemer LS, Lee WM, Feldman MD and Sehgal CM: The antivasular action of physiotherapy ultrasound on murine tumors. *Ultrasound Med Biol* 31: 1403-1410, 2005.
29. Chen H, Brayman AA, Bailey MR and Matula TJ: Blood vessel rupture by cavitation. *Urol Res* 38: 321-326, 2010.
30. Ahmadi F, McLoughlin IV, Chauhan S and ter-Haar G: Bio-effects and safety of low-intensity, low-frequency ultrasonic exposure. *Prog Biophys Mol Biol* 108: 119-138, 2012.
31. Polat BE, Hart D, Langer R and Blankschtein D: Ultrasound-mediated transdermal drug delivery: Mechanisms, scope and emerging trends. *J Control Release* 152: 330-348, 2011.
32. Carvell KJ and Bigelow TA: Dependence of optimal seed bubble size on pressure amplitude at therapeutic pressure levels. *Ultrasonics* 51: 115-122, 2011.
33. Stride EP and Coussios CC: Cavitation and contrast: The use of bubbles in ultrasound imaging and therapy. *Proc Inst Mech Eng H* 224: 171-191, 2010.
34. Hosseinkhah N and Hynynen K: A three-dimensional model of an ultrasound contrast agent gas bubble and its mechanical effects on microvessels. *Phys Med Biol* 57: 785-808, 2012.
35. VanBavel E: Effects of shear stress on endothelial cells: Possible relevance for ultrasound applications. *Prog Biophys Mol Biol* 93: 374-383, 2007.
36. Dayton P, Klivanov A, Brandenburger G and Ferrara K: Acoustic radiation force in vivo: A mechanism to assist targeting of microbubbles. *Ultrasound Med Biol* 25: 1195-1201, 1999.
37. Basta G, Venneri L, Lazzerini G, Pasanisi E, Pianelli M, Vesentini N, Del Turco S, Kusmic C and Picano E: In vitro modulation of intracellular oxidative stress of endothelial cells by diagnostic cardiac ultrasound. *Cardiovasc Res* 58: 156-161, 2003.
38. Chen H, Brayman AA, Kreider W, Bailey MR and Matula TJ: Observations of translation and jetting of ultrasound-activated microbubbles in mesenteric microvessels. *Ultrasound Med Biol* 37: 2139-2148, 2011.
39. Coralic V and Colonius T: Shock-induced collapse of a bubble inside a deformable vessel. *Eur J Mech B Fluids* 40: 64-74, 2013.
40. Chen H, Kreider W, Brayman AA, Bailey MR and Matula TJ: Blood vessel deformations on microsecond time scales by ultrasonic cavitation. *Phys Rev Lett* 106: 034301, 2011.
41. Gao F, Xiong C and Xiong Y: Constrained oscillation of a bubble subjected to shock wave in microvessel. *Prog Nat Sci* 19: 1109-1117, 2009.
42. Ke S, Ding XM, Kong J, Gao J, Wang SH, Cheng Y and Sun WB: Low temperature of radiofrequency ablation at the target sites can facilitate rapid progression of residual hepatic VX2 carcinoma. *J Transl Med* 8: 73, 2010.
43. Nijkamp MW, van der Bilt JD, de Bruijn MT, Molenaar IQ, Voest EE, van Diest PJ, Kranenburg O and Borel Rinkes IH: Accelerated perinecrotic outgrowth of colorectal liver metastases following radiofrequency ablation is a hypoxia-driven phenomenon. *Ann Surg* 249: 814-823, 2009.
44. Ruan K, Song G and Ouyang G: Role of hypoxia in the hallmarks of human cancer. *J Cell Biochem* 107: 1053-1062, 2009.